Peer-reviewed version available at Nanomaterials 2018, 8, 725; doi:10.3390/nano8090725

Thickness-dependent differential reflectance spectra of monolayer and few-layer MoS_2, $MoSe_2$, WS_2 and WSe_2

*Yue Niu[1,2], Sergio Gonzalez-Abad[1], Riccardo Frisenda[3], Philipp Marauhn[4], Matthias Drüppel[4], Patricia Gant[3], Robert Schmidt[5], Najme S. Taghavi,[3,6] David Barcons,[5] Aday J. Molina-Mendoza,[7] Steffen Michaelis de Vasconcellos[5], Rudolf Bratschitsch[5], David Perez De Lara[1], Michael Rohlfing[4], Andres Castellanos-Gomez[3,]**

[1] *Instituto Madrileño de Estudios Avanzados en Nanociencia (IMDEA Nanociencia), Campus de Cantoblanco, E-28049 Madrid, Spain.*

[2] *National Key Laboratory of Science and Technology on Advanced Composites in Special Environments, Harbin Institute of Technology, Harbin, China.*

[3] *Materials Science Factory, Instituto de Ciencia de Materiales de Madrid (ICMM), Consejo Superior de Investigaciones Científicas (CSIC), Sor Juana Inés de la Cruz 3, 28049 Madrid, Spain.*

[4] *Institute of Solid-state Theory, University of Münster, 48149 Münster, Germany.*

[5] *Institute of Physics and Center for Nanotechnology, University of Münster, 48149 Münster, Germany*

[6] *Khaje Nasir Toosi University of Technology (KNTU), Faculty of Physics, Tehrān, Iran*

[7] *Institute of Photonics (Vienna University of Technology), Gusshausstrasse 27-29, 1040 Vienna, Austria.*

andres.castellanos@csic.es

The research field of two dimensional (2D) materials strongly relies on optical microscopy characterization tools to identify atomically thin materials and to determine their number of layers. Moreover, optical microscopy-based techniques also opened the door to study the optical properties of these nanomaterials. We present a comprehensive study of the differential reflectance spectra of 2D semiconducting transition metal dichalcogenides (TMDCs), MoS_2, $MoSe_2$, WS_2 and WSe_2, with thickness ranging from one layer up to six layers. We analyze the thickness-dependent energy of the different excitonic features, indicating the change in the band structure of the different TMDC materials with the number of layers. Our work provides a route to employ differential reflectance spectroscopy for determining the number of layers of MoS_2, $MoSe_2$, WS_2 and WSe_2.

The isolation of atomically thin semiconducting TMDCs by mechanical exfoliation of bulk layered crystals has aroused the interest of the nanoscience and nanotechnology

community on these 2D semiconductors.[1–5] These materials have a band gap within the visible part of the spectrum, bridging the gap between graphene (zero-gap semiconductor) and hexagonal boron nitride (wide-gap semiconductor). Recently, the band gap of semiconductor TMDCs has been exploited to fabricate optoelectronic devices such as photodetectors [6–12] and solar cells.[13–17] Photoluminescence studies also demonstrated that a reduction in thickness has a strong effect on the band structure of MoS_2 and other semiconductor TMDCs.[18–20] However, the determination of the intrinsic quantum efficiency and the photoresponse of photodetectors based on semiconducting TMDCs requires of a comprehensive study of their reflectance and/or transmittance with different number of layers in a wide spectral range, which is still lacking.

Here we systematically study the differential reflectance of single- and few-layer MoS_2, $MoSe_2$, WS_2 and WSe_2 from the near-infrared (1.4 eV) to the near-ultraviolet (3.0 eV). The differential reflectance spectra show prominent features due to excitons. The thickness dependence of these excitonic features is analyzed.

Single- and few-layer MoS_2, $MoSe_2$, WS_2 and WSe_2 samples are fabricated by mechanical exfoliation of bulk layered crystals onto a polydimethil-siloxane (PDMS) substrate (Gelfilm from Gelpak®[21]; see the Supporting Information for results obtained with other substrates). We address the reader to the Materials and Methods section for more details about the sample fabrication. Also note that all results shown in the main text are obtained for the 2H polytype, which is the most common for this family of materials. We address the reader to the Supporting Information for a comparison between the 2H- and 3R-MoS_2 polytypes.

Figure 1a shows a transmission mode optical microscopy image of an exfoliatedMoS_2 flake displaying regions with different number of layers, as determined from the position of the E_{2g} and A_{1g} lines in their Raman spectra (Figure 1b).[22,23] Similar optical microscopy images of $MoSe_2$, WS_2 and WSe_2 samples can be found in the Supporting Information. The quantitative analysis of the red, green and blue channels of the transmission mode optical images has been recently proven to be a effective alternative way to determine the number of layers of TMDCs (see Ref. [24] and the Supporting Information in Ref.[25]). Figure 1c shows the transmittance T/T_0 (T: intensity of the light transmitted through the flake, T_0: intensity of the light transmitted through the substrate) extracted from the different regions of the transmission mode optical image shown in Figure 1a. The blue channel shows the largest thickness dependence. Thus it can be very useful to determine the number of layers. The blue channel transmittance drops monotonically by ~9% per MoS_2 layer, in good agreement with the results reported in Ref. [24]. We have found that the blue channel transmittance also shows a strong thickness dependence for other TMDCs studied here: WS_2, WSe_2 or $MoSe_2$ (see the Supporting Information for an analogue of Figure 1c for these materials). This strong thickness dependence of the blue channel transmittance might be especially relevant to determine the number of layers of relatively thick MoS_2 multilayers, as Raman spectroscopy is only accurate to determine layers thinner than 4 layers (the Raman shift difference between the E_{2g} and A_{1g} quickly saturates for flakes thicker than 4 layers, see Ref. [22]). Furthermore, for WS_2, WSe_2 or $MoSe_2$ it is not trivial to determine the number of layers with Raman spectroscopy as one might need a high resolution Raman system or a system capable to resolve shear Raman modes occurring at low Raman shifts [26–31] (see the Supporting Information to see the thickness dependent Raman spectra of WS_2, WSe_2 or $MoSe_2$).

The optical spectra of the fabricated flakes are characterized by using a homebuilt micro-reflectance and transmittance setup. We address the reader to References [32,33] for details on this experimental setup. Briefly, the setup consists of a Motic BA310 metallurgical microscope supplemented with a modified trinocular port that sends part of the reflected light to a fiber-coupled CCD spectrometer to be analyzed. The system can be used to measure differential reflectance and transmittance. In the main text, we show the results of differential reflectance measurements and we address the reader to the Supporting Information for a comparison between differential reflectance and transmittance measurements acquired on the same sample.

The differential reflectance spectrum is calculated as $(R\text{-}R_0)/R$ and it is related to the absorption coefficient of the material $\alpha(\lambda)$ as[34,35]

$$\frac{R - R_0}{R} = \frac{4n}{{n_0}^2 - 1}\alpha(\lambda)$$

where R is the intensity reflected by the flake, R_0 the intensity reflected by the substrate, n is the refractive index of the flake under study and n_0 is the refractive index of the substrate. Figure 2 shows the differential reflectance spectra measured on the single- and few-layer regions for the different semiconductor TMDCs studied here. The spectra acquired for this family of 2D materials show overall similar features: pronounced peaks corresponding to the generation of excitons. The exact energy at which these peaks appear is material-to-material dependent because those features are determined by the band structures of these different compounds. The exciton peaks in Figure 2 are labelled A, B and C (and D for WSe_2) following the nomenclature employed in the literature to name the different excitons in semiconducting TMDCs.[18–20] The A exciton, occurring near the absorption band edge, corresponds to direct band gap transitions at the *K* point in the Brillouin zone.[18–20] This feature is the most studied one, as it is also the dominant one

Peer-reviewed version available at Nanomaterials 2018, 8, 725; doi:10.3390/nano8090725

in photoluminescence spectra. Close to the A exciton peak, at slightly higher energy, the transition metal dichalcogenides show another prominent peak in their differential reflectance spectra, corresponding to another direct band gap transition at the *K* point but at higher energy that yields the creation of the so-called B excitons. For monolayer TMDCs, the origin of this higher energy transition at the *K* point is related to the splitting of the valence band due to the spin-orbit interaction. For multilayer systems, the splitting of the valence band is driven by a combination of spin-orbit- and interlayer interaction.

Apart from the narrow A and B exciton peaks, the differential reflectance spectra of MoS_2, $MoSe_2$ and WS_2 also show other broader spectroscopic features in an energy range from 2.5 eV to 2.9 eV (referred to as C exciton peak), which is due to singularities in the joint density of states between the first valence and conduction bands in a circle around the Γ point (into the local minimum of the lowest conduction band between Γ and *K*) that leads to multiple optical transitions nearly degenerate in energy.[34,36–41] For WSe_2, we find instead of just one broad C exciton feature, two features labeled C and D as were also reported in recent absorption measurements.[41] While the C exciton of WSe_2 consists of several transitions along the Γ-*K* direction between the highest valence and lowest conduction bands, the D exciton has largest contributions from the spin-split lower valence band into the lowest conduction band [41].

The differential reflectance spectra have been fit to a sum of Gaussian/Lorentzian peaks with a broad background to determine the peak position, width and magnitude of the excitonic features as a function of the number of layers for the different 2D semiconductor materials. The thin black lines in Figure 3 correspond to the resulting fits for the different measured spectra and the empty circles highlight the energy value determined for the different excitons from the fits. In order to visualize the thickness dependence of the exciton energies, Figure 3 summarizes the determined exciton energies as a function of

Peer-reviewed version available at Nanomaterials 2018, 8, 725; doi:10.3390/nano8090725

the number of layers for MoS_2, $MoSe_2$, WS_2 and WSe_2. The A exciton peak redshifts as the thickness increases for all the studied materials, in agreement with previous photoluminescence results. The B exciton, however, shows moderate thickness dependence. As discussed above, for single layers the separation between the A and B exciton peaks is due to the spin-orbit splitting of the valence band. Therefore, the larger spin-orbit splitting induced by the heavier W atoms with respect to Mo atoms, is translated to a larger separation of the A and B features in the differential reflectance spectra of W-based TMDCs. Also, Se- based dichalcogenides exhibit a larger splitting between the A and B exciton peaks than that of S- based dichalcogenides. Table 1 summarizes the values of the splitting between the A and B excitons for the single-layer TMDCs studied in this work, and compares these values with theoretical values obtained through *ab initio* calculations (see the Supporting Information for more details about the calculations).

Material	Experimental A-B splitting (meV)	Theoretical A-B splitting (meV)
1L – MoS_2	124 ± 5	152
1L – $MoSe_2$	219 ± 10	218
1L – WS_2	371 ± 5	420
1L – WSe_2	398 ± 10	464

Table 1. Comparison of the spin-orbit splitting extracted from the differential reflectance spectra and those obtained from *ab initio* calculations including spin-orbit interaction.

Interestingly, we also find that the C exciton shows a prominent shift with the thickness, even more pronounced than that of the A exciton. Note that the number of works studying the C excitonic feature are still very scarce as most experiments employ photoluminescence with green laser excitation (E ~2 eV - 2.3 eV) to observe the generated excitons.

Peer-reviewed version available at Nanomaterials 2018, 8, 725; doi:10.3390/nano8090725

In summary, we presented a systematic study of the differential reflectance spectra MoS_2, $MoSe_2$, WS_2 and WSe_2 from the near-infrared (1.4 eV) to the near-ultraviolet (3.0 eV). The differential reflectance spectra show prominent features due to the generation of excitons and the energy at which these features appear depends on the thickness of the flakes because of quantum confinement effects. We propose to employ a combination of a quantitative analysis of transmission mode optical images and differential reflectance measurements to be used as an alternative method to determine the number of layers.

MATERIALS AND METHODS

We prepared MoS_2, $MoSe_2$, WS_2 and WSe_2 nanosheets by mechanical exfoliation with blue Nitto tape (Nitto Denko Co., SPV 224P) on a commercially available polydimethil-siloxane substrates (Gel-Film from Gelpak®). $MoSe_2$, WS_2 and WSe_2 bulk crystals were synthetic (grown by vapor transport method), while the MoS_2 material employed in this work is a naturally occurring molybdenite crystal (Moly Hill mine, Quebec, Canada). All the materials studied in the main text were 2H polytype. In the Supporting Information we also include results obtained for mechanically exfoliated natural 3R-MoS_2 (Mont St. Hilaire, Quebec, Canada). Few-layer flakes are identified under an optical microscope (Nikon Eclipse CI) and the number of layers is determined by their opacity in transmission mode. The optical properties of the nanosheets have been studied with a home-built micro-reflectance/transmittance setup, described in detail in Ref. [32].

The calculations of the absorption spectra were conducted using the *GW*-BSE method within the LDA+*GdW* approximation[42]. Here, the dielectric screening is implemented by an atom-resolved model function based on the random phase approximation. For the structural parameters, we used the experimental values as reported in Ref.[43] (with $a =$

3.160 Å for MoS_2 and $a = 3.299$ Å for $MoSe_2$) and Ref.[44] (with $a = 3.155$ Å for WS_2 and $a = 3.286$ Å for WSe_2). We start with a DFT calculation within the LDA, using a basis set of localized Gaussian orbitals and norm-conserving pseudopotentials that also include spin-orbit interaction. The resulting wave functions and energies are used for a subsequent *GdW* calculation, fully taking into account spin-orbit interaction. For the BSE calculations, we use a $24 \times 24 \times 1$ k-point grid for the mono- and bilayers and an $18 \times 18 \times 3$ k-point grid for the bulk crystals. Notably, we use identical meshes both for the quasiparticle corrections and the electron-hole interaction, so no interpolation scheme is needed. The number of valence and conduction bands in the BSE Hamiltonian were doubled when going from the monolayer (four/six) to the bilayer and bulk crystals (eight/twelve). A detailed analysis of the convergence of the presented calculation is found in the Supporting Information. For all absorption spectra, an artificial broadening of 35 meV is applied.

Author contributions

YN, SGA, PG, AMM, RF, NT, DB, DPdL and ACG fabricated the samples, performed the optical spectroscopy measurements and analyzed the experimental results. RS, SMdV and RB provided the bulk $MoSe_2$, WS_2 and WSe_2 crystals. PM, MD and MR performed the ab-initio calculations. All the authors discussed the results and contributed in the elaboration of the manuscript.

ACKNOWLEDGMENT

We thank Prof. Emilio M. Pérez for his support with the Raman spectroscopy measurements. This project has received funding from the European Research Council (ERC) under the European Union's Horizon 2020 research and innovation programme (grant agreement n° 755655, ERC-StG 2017 project 2D-TOPSENSE). ACG and PG acknowledge funding from the EU Graphene Flagship funding (Grant Graphene Core 2,

785219). RF acknowledges support from the Netherlands Organisation for Scientific Research (NWO) through the research program Rubicon with project number 680-50-1515. DPdL acknowledges support from the MINECO (program FIS2015-67367-C2-1-P). YN acknowledges the grant from the China Scholarship Council (File NO. 201506120102). PM, MD, and MR gratefully acknowledge the computing time granted by the John von Neumann Institute for Computing (NIC) and provided on the super-computer JURECA at Jülich Supercomputing Centre (JSC)

REFERENCES

[1] Novoselov K S, Jiang D, Schedin F, Booth T J, Khotkevich V V, Morozov S V and Geim a K 2005 Two-dimensional atomic crystals. *Proc. Natl. Acad. Sci. U. S. A.* **102** 10451–3

[2] Xu M, Liang T, Shi M and Chen H 2013 Graphene-like two-dimensional materials. *Chem. Rev.* **113** 3766–98

[3] Xia F, Wang H, Xiao D, Dubey M and Ramasubramaniam A 2014 Two-dimensional material nanophotonics *Nat. Photonics* **8** 899–907

[4] Lv R, Robinson J A, Schaak R E, Sun D, Sun Y, Mallouk T E and Terrones M 2015 Transition Metal Dichalcogenides and Beyond: Synthesis, Properties, and Applications of Single- and Few-Layer Nanosheets. *Acc. Chem. Res.* **48** 56–64

[5] Wang Q H, Kalantar-Zadeh K, Kis A, Coleman J N and Strano M S 2012 Electronics and optoelectronics of two-dimensional transition metal dichalcogenides. *Nat. Nanotechnol.* **7** 699–712

[6] Yin Z, Li H, Li H, Jiang L, Shi Y, Sun Y, Lu G, Zhang Q, Chen X and Zhang H 2012 Single-layer MoS2 phototransistors. *ACS Nano* **6** 74–80

[7] Lee H S, Min S-W, Chang Y-G, Park M K, Nam T, Kim H, Kim J H, Ryu S and Im S 2012 MoS nanosheet phototransistors with thickness-modulated optical energy gap. *Nano Lett.* **12** 3695–700

[8] Zhang W, Chiu M-H, Chen C-H, Chen W, Li L-J and Wee A T S 2014 Role of metal contacts in high-performance phototransistors based on WSe2 monolayers. *ACS Nano* **8** 8653–61

[9] Choi W, Cho M Y, Konar A, Lee J H, Cha G-B, Hong S C, Kim S, Kim J, Jena D, Joo J and Kim S 2012 High-detectivity multilayer MoS(2) phototransistors with spectral response from ultraviolet to infrared. *Adv. Mater.* **24** 5832–6

[10] Zhang W, Huang J-K, Chen C-H, Chang Y-H, Cheng Y-J and Li L-J 2013 High-gain phototransistors based on a CVD MoS monolayer. *Adv. Mater.* **25** 3456–61

[11] Abderrahmane A, Ko P J, Thu T V, Ishizawa S, Takamura T and Sandhu A 2014 High photosensitivity few-layered MoSe2 back-gated field-effect phototransistors. *Nanotechnology* **25** 365202

[12] Lopez-Sanchez O, Lembke D, Kayci M, Radenovic A and Kis A 2013 Ultrasensitive photodetectors based on monolayer MoS2 *Nat. Nanotechnol.* **8** 497–501

[13] Ross J S, Klement P, Jones A M, Ghimire N J, Yan J, Mandrus D G, Taniguchi T, Watanabe K, Kitamura K, Yao W, Cobden D H and Xu X 2014 Electrically tunable excitonic light-emitting diodes based on monolayer WSe2 p-n junctions. *Nat. Nanotechnol.* **9** 268–72

[14] Baugher B W H, Churchill H O H, Yang Y and Jarillo-Herrero P 2014 Optoelectronic devices based on electrically tunable p-n diodes in a monolayer dichalcogenide. *Nat. Nanotechnol.* **9** 262–7

[15] Pospischil A, Furchi M M and Mueller T 2014 Solar-energy conversion and light emission in an atomic monolayer p-n diode. *Nat. Nanotechnol.* **9** 257–61

[16] Lee C-H, Lee G-H, van der Zande A M, Chen W, Li Y, Han M, Cui X, Arefe G, Nuckolls C, Heinz T F, Guo J, Hone J and Kim P 2014 Atomically thin p–n junctions with van der Waals heterointerfaces *Nat. Nanotechnol.* **9** 676–81

[17] Groenendijk D J, Buscema M, Steele G A, Michaelis de Vasconcellos S, Bratschitsch R,

van der Zant H S J and Castellanos-Gomez A 2014 Photovoltaic and photothermoelectric effect in a double-gated WSe2 device. *Nano Lett.* **14** 5846–52

[18] Splendiani A, Sun L, Zhang Y, Li T, Kim J, Chim C-Y, Galli G and Wang F 2010 Emerging photoluminescence in monolayer MoS2 *Nano Lett.* **10** 1271–5

[19] Mak K F, Lee C, Hone J, Shan J and Heinz T F 2010 Atomically Thin MoS_{2}: A New Direct-Gap Semiconductor *Phys. Rev. Lett.* **105** 136805

[20] Zhao W, Ghorannevis Z, Chu L, Toh M, Kloc C, Tan P-H and Eda G 2013 Evolution of electronic structure in atomically thin sheets of WS2 and WSe2. *ACS Nano* **7** 791–7

[21] Buscema M, Steele G A, van der Zant H S J and Castellanos-Gomez A 2014 The effect of the substrate on the Raman and photoluminescence emission of single-layer MoS2 *Nano Res.* **7** 561–71

[22] Lee C, Yan H, Brus L E, Heinz T F, Hone Ḱ J and Ryu S 2010 Anomalous Lattice Vibrations of Single-and Few-Layer MoS2 *ACS Nano* **4** 2695–700

[23] Placidi M, Dimitrievska M, Izquierdo-Roca V, Fontané X, Castellanos-Gomez A, Pérez-Tomás A, Mestres N, Espindola-Rodriguez M, López-Marino S and Neuschitzer M 2015 Multiwavelength excitation Raman scattering analysis of bulk and two-dimensional MoS2: vibrational properties of atomically thin MoS2 layers *2D Mater.* **2** 35006

[24] Zhang H, Ran F, Shi X, Fang X, Wu S, Liu Y, Zheng X, Yang P, Liu Y, Wang L, Huang X, Li H and Huang W 2017 Optical thickness identification of transition metal dichalcogenide nanosheets on transparent substrates *Nanotechnology* **28** 164001

[25] Castellanos-Gomez A, Roldán R, Cappelluti E, Buscema M, Guinea F, van der Zant H S J and Steele G A 2013 Local strain engineering in atomically thin MoS2. *Nano Lett.* **13** 5361–6

[26] Plechinger G, Heydrich S, Eroms J, Weiss D, Schüller C and Korn T 2012 Raman spectroscopy of the interlayer shear mode in few-layer MoS 2 flakes *Appl. Phys. Lett.* **101** 101906

[27] Zhao W, Ghorannevis Z, Amara K K, Pang J R, Toh M, Zhang X, Kloc C, Tan P H and Eda G 2013 Lattice dynamics in mono-and few-layer sheets of WS 2 and WSe 2 *Nanoscale* **5** 9677–83

[28] Zhang X, Han W P, Wu J B, Milana S, Lu Y, Li Q Q, Ferrari A C and Tan P H 2013 Raman spectroscopy of shear and layer breathing modes in multilayer MoS 2 *Phys. Rev. B* **87** 115413

[29] Zhao Y, Luo X, Li H, Zhang J, Araujo P T, Gan C K, Wu J, Zhang H, Quek S Y and Dresselhaus M S 2013 Interlayer breathing and shear modes in few-trilayer MoS2 and WSe2 *Nano Lett.* **13** 1007–15

[30] Tonndorf P, Schmidt R, Böttger P, Zhang X, Börner J, Liebig A, Albrecht M, Kloc C, Gordan O, Zahn D R T, Michaelis de Vasconcellos S and Bratschitsch R 2013 Photoluminescence emission and Raman response of monolayer MoS_2, MoSe_2, and WSe_2 *Opt. Express* **21** 4908

[31] Puretzky A A, Liang L, Li X, Xiao K, Wang K, Mahjouri-Samani M, Basile L, Idrobo J C, Sumpter B G and Meunier V 2015 Low-frequency Raman fingerprints of two-dimensional metal dichalcogenide layer stacking configurations *ACS Nano* **9** 6333–42

[32] Frisenda R, Niu Y, Gant P, Molina-Mendoza A J, Schmidt R, Bratschitsch R, Liu J, Fu L, Dumcenco D, Kis A, Perez De Lara D and Castellanos-Gomez A 2017 Micro-reflectance and transmittance spectroscopy: a versatile and powerful tool to characterize 2D materials *J. Phys. D. Appl. Phys.* **50** 74002

[33] Ghasemi F, Frisenda R, Dumcenco D, Kis A, Perez de Lara D and Castellanos-Gomez A 2017 High Throughput Characterization of Epitaxially Grown Single-Layer MoS2

Electronics **6** 28

[34] Dhakal K P, Duong D L, Lee J, Nam H, Kim M, Kan M, Lee Y H and Kim J 2014 Confocal absorption spectral imaging of MoS2: optical transitions depending on the atomic thickness of intrinsic and chemically doped MoS2. *Nanoscale* **6** 13028–35

[35] McIntyre J D E and Aspnes D E 1971 Differential reflection spectroscopy of very thin surface films *Surf. Sci.* **24** 417–34

[36] Qiu D Y, da Jornada F H and Louie S G 2013 Optical Spectrum of MoS 2 : Many-Body Effects and Diversity of Exciton States *Phys. Rev. Lett.* **111** 216805

[37] Kozawa D, Kumar R, Carvalho A, Kumar Amara K, Zhao W, Wang S, Toh M, Ribeiro R M, Castro Neto A H, Matsuda K and Eda G 2014 Photocarrier relaxation pathway in two-dimensional semiconducting transition metal dichalcogenides *Nat. Commun.* **5** 193–335

[38] Klots A R, Newaz A K M, Wang B, Prasai D, Krzyzanowska H, Lin J, Caudel D, Ghimire N J, Yan J, Ivanov B L, Velizhanin K A, Burger A, Mandrus D G, Tolk N H, Pantelides S T and Bolotin K I 2014 Probing excitonic states in suspended two-dimensional semiconductors by photocurrent spectroscopy. *Sci. Rep.* **4** 6608

[39] Castellanos-Gomez A, Quereda J, van der Meulen H P, Agraït N and Rubio-Bollinger G 2016 Spatially resolved optical absorption spectroscopy of single- and few-layer MoS 2 by hyperspectral imaging *Nanotechnology* **27** 115705

[40] Gibaja C, Rodriguez-San-Miguel D, Ares P, Gómez-Herrero J, Varela M, Gillen R, Maultzsch J, Hauke F, Hirsch A, Abellán G and Zamora F 2016 Few-Layer Antimonene by Liquid-Phase Exfoliation *Angew. Chemie Int. Ed.*

[41] Schmidt R, Niehues I, Schneider R, Drüppel M, Deilmann T, Rohlfing M, de Vasconcellos S M, Castellanos-Gomez A and Bratschitsch R 2016 Reversible uniaxial strain tuning in atomically thin WSe2 *2D Mater.* **3** 21011

[42] Rohlfing M 2010 Electronic excitations from a perturbative LDA + G d W approach *Phys. Rev. B* **82** 205127

[43] Böker T, Severin R, Müller A, Janowitz C, Manzke R, Voß D, Krüger P, Mazur A and Pollmann J 2001 Band structure of MoS 2 , MoSe 2 , and α − MoTe 2 : Angle-resolved photoelectron spectroscopy and *ab initio* calculations *Phys. Rev. B* **64** 235305

[44] Yun W S, Han S W, Hong S C, Kim I G and Lee J D 2012 Thickness and strain effects on electronic structures of transition metal dichalcogenides: 2H- M X 2 semiconductors (M = Mo, W; X = S, Se, Te) *Phys. Rev. B* **85** 33305

[45] Castellanos-Gomez A, Buscema M, Molenaar R, Singh V, Janssen L, van der Zant H S J and Steele G A 2014 Deterministic transfer of two-dimensional materials by all-dry viscoelastic stamping *2D Mater.* **1** 11002

[46] Blake P, Hill E W, Castro Neto A H, Novoselov K S, Jiang D, Yang R, Booth T J and Geim A K 2007 Making graphene visible *Appl. Phys. Lett.* **91** 63124

[47] Abergel D S L, Russell A and Fal'ko V I 2007 Visibility of graphene flakes on a dielectric substrate *Appl. Phys. Lett.* **91** 63125

[48] Roddaro S, Pingue P, Piazza V, Pellegrini V and Beltram F 2007 The optical visibility of graphene: interference colors of ultrathin graphite on SiO(2). *Nano Lett.* **7** 2707–10

[49] Castellanos-Gomez A, Agraït N and Rubio-Bollinger G 2010 Optical identification of atomically thin dichalcogenide crystals *Appl. Phys. Lett.* **96** 213116

[50] Benameur M M, Radisavljevic B, Héron J S, Sahoo S, Berger H and Kis a 2011 Visibility of dichalcogenide nanolayers. *Nanotechnology* **22** 125706

[51] Li H, Lu G, Yin Z, He Q, Li H, Zhang Q and Zhang H 2012 Optical Identification of

Single- and Few-Layer MoS2 Sheets *Small* **8** 682–6

[52] Li H, Wu J, Huang X, Lu G, Yang J, Lu X, Xiong Q and Zhang H 2013 Rapid and reliable thickness identification of two-dimensional nanosheets using optical microscopy. *ACS Nano* **7** 10344–53

[53] Rubio-Bollinger G, Guerrero R, Pérez de Lara D, Quereda J, Vaquero-Garzon L, Agraït N, Bratschitsch R and Castellanos-Gomez A 2015 Enhanced Visibility of MoS2, MoSe2, WSe2 and Black-Phosphorus: Making Optical Identification of 2D Semiconductors Easier *Electronics* **4** 847–56

FIGURES:

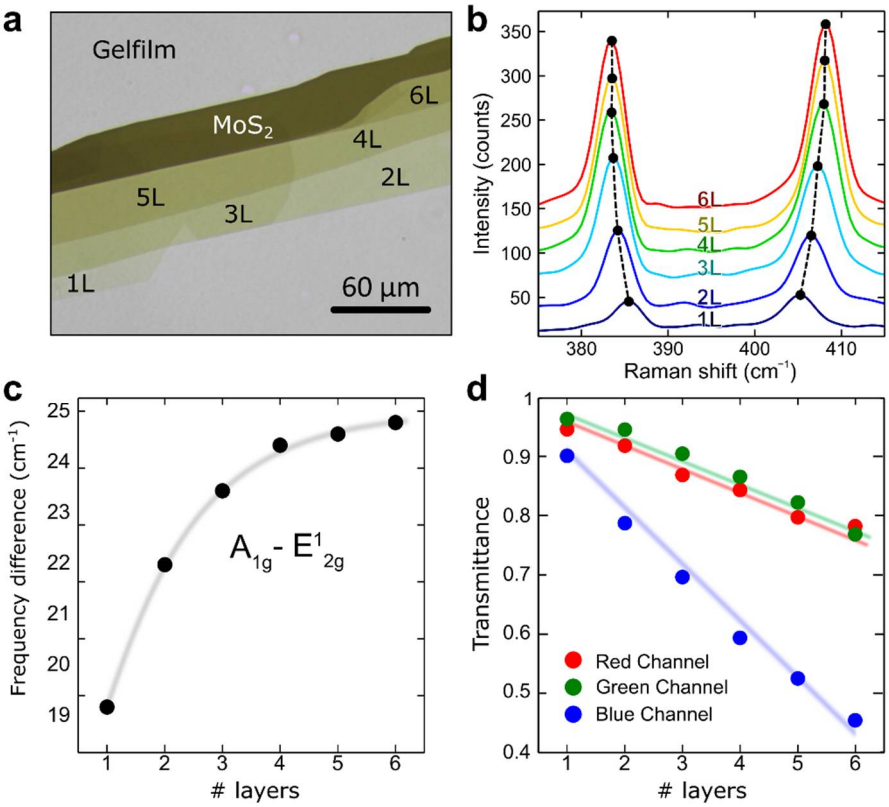

Figure1. (a) Transmission mode optical image of a mechanically exfoliated MoS_2 flake on PDMS substrate. (b) Raman spectra measured on the different regions of the flakes. The thickness of

the flake can be determined from the Raman shift difference between the A1g and E2g lines, shown in panel (c). (d) Transmittance of the MoS_2 flake (extracted from the red, green and blue channels of the trasnmission mode optical images) as a function of the number of layers.

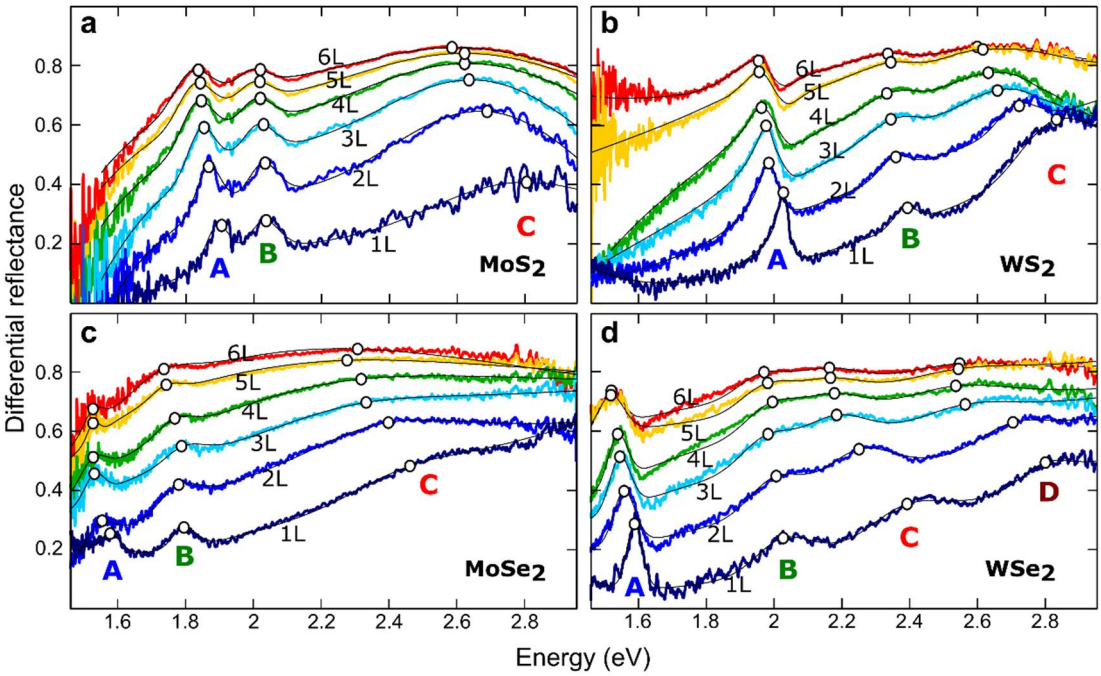

Figure 2. Differential reflectance spectra measured as a function of the number of layers for (a) MoS_2, (b) WS_2, (c) $MoSe_2$ and (d) WSe_2. The spectra have been fitted to a sum of Lorentzian/Gaussian peaks (solid thin black lines) to determine the position of the different excitonic features (highlighted with white circles).

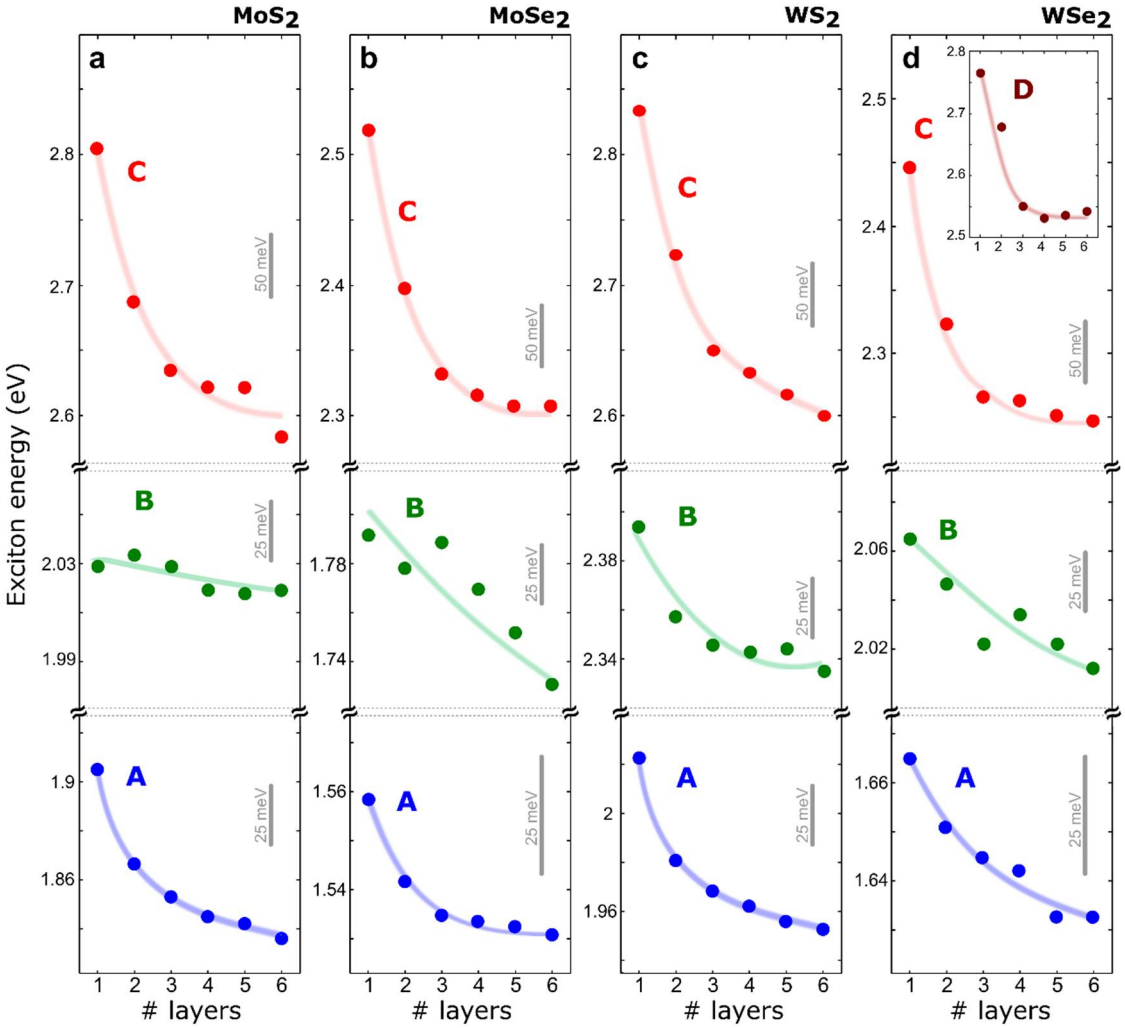

Figure 3. Thickness dependence of the exciton energies, extracted from the measured differential reflectance spectra of (a) MoS_2, (b) WS_2, (c) $MoSe_2$ and (d) WSe_2. The solid lines are guides to the eye.

Peer-reviewed version available at Nanomaterials 2018, 8, 725; doi:10.3390/nano8090725

Supporting information:

Thickness-dependent optical properties of monolayer and few-layer MoS_2, $MoSe_2$, WS_2 and WSe_2

*Yue Niu[1,2], Sergio Gonzalez-Abad[1], Riccardo Frisenda[3], Philipp Marauhn[4], Matthias Drüppel[4], Patricia Gant[3], Robert Schmidt[5], Najme S. Taghavi,[3,6] David Barcons,[5] Aday J. Molina-Mendoza,[7] Steffen Michaelis de Vasconcellos[5], Rudolf Bratschitsch[5], David Perez De Lara[1], Michael Rohlfing[4], Andres Castellanos-Gomez[3,]**

[1] *Instituto Madrileño de Estudios Avanzados en Nanociencia (IMDEA Nanociencia), Campus de Cantoblanco, E-28049 Madrid, Spain.*

[2] *National Key Laboratory of Science and Technology on Advanced Composites in Special Environments, Harbin Institute of Technology, Harbin, China.*

[3] *Materials Science Factory, Instituto de Ciencia de Materiales de Madrid (ICMM), Consejo Superior de Investigaciones Científicas (CSIC), Sor Juana Inés de la Cruz 3, 28049 Madrid, Spain.*

[4] *Institute of Solid-state Theory, University of Münster, 48149 Münster, Germany.*

[5] *Institute of Physics and Center for Nanotechnology, University of Münster, 48149 Münster, Germany*

[6] *Khaje Nasir Toosi University of Technology (KNTU), Faculty of Physics, Tehrān, Iran*

[7] *Institute of Photonics (Vienna University of Technology), Gusshausstrasse 27-29, 1040 Vienna, Austria.*

andres.castellanos@csic.es

Preprints (www.preprints.org) | NOT PEER-REVIEWED | Posted: 14 August 2018 doi:10.20944/preprints201808.0242.v1

Peer-reviewed version available at Nanomaterials 2018, 8, 725; doi:10.3390/nano8090725

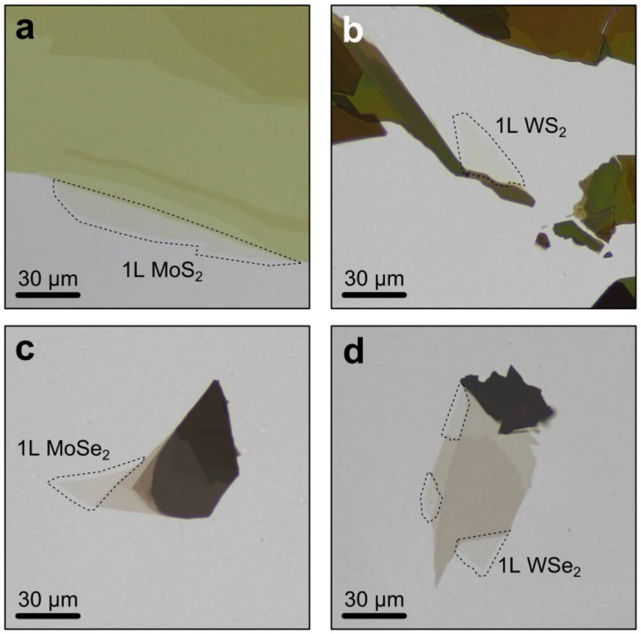

Figure S1. Transmission mode optical images of mechanically exfoliated TMDCs onto PDMS substrates. (a) MoS_2. (b) WS_2. (c) $MoSe_2$. (d) WSe_2. Single-layer areas have been highlighted with a dashed black line.

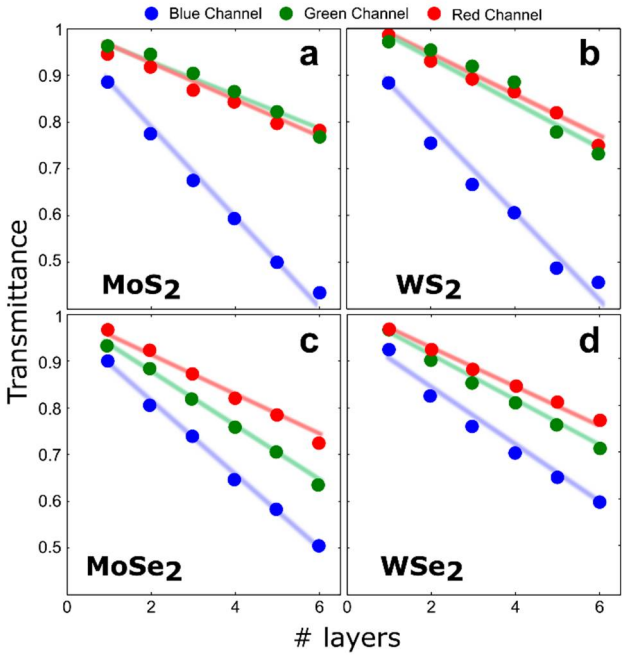

Figure S2. Trasmittance (extracted from the red, green and blue channels of the trasnmission mode optical images) as a function of the number of layers. (a) MoS_2. (b) WS_2. (c) $MoSe_2$. (d) WSe_2. The solid lines are guides to the eye.

Peer-reviewed version available at Nanomaterials 2018, 8, 725; doi:10.3390/nano8090725

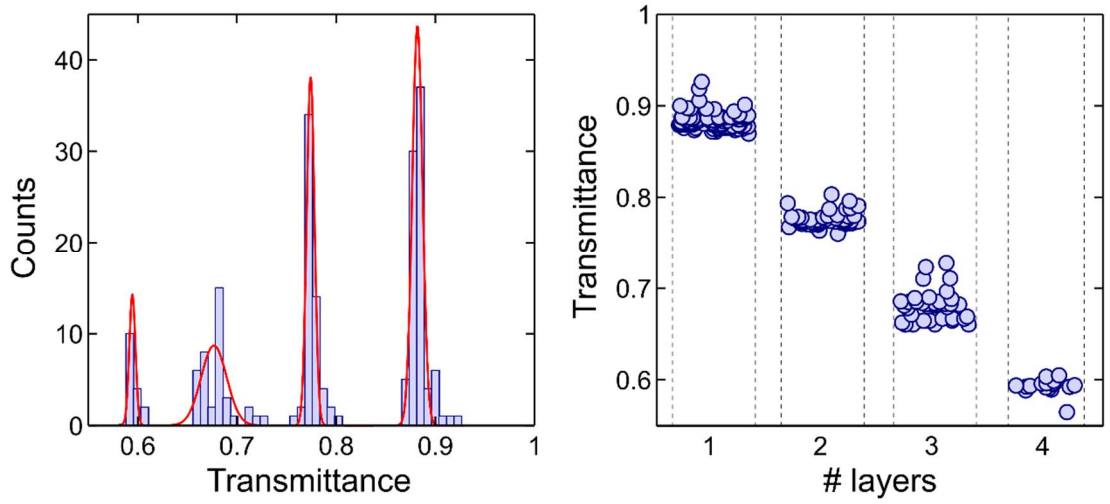

Figure S3. (a) Histogram of the blue channel transmittance measured on more than 200 MoS_2 flakes with different number of layers (ranging from 1 layer to 4 layers). The histogram has been fitted to a sum of 4 Gaussian curves. (b) Number of layers assigned from the transmittance of the blue channel of the same Mos_2 flakes shown in (a).

Preprints (www.preprints.org) | NOT PEER-REVIEWED | Posted: 14 August 2018 doi:10.20944/preprints201808.0242.v1

Peer-reviewed version available at Nanomaterials 2018, 8, 725; doi:10.3390/nano8090725

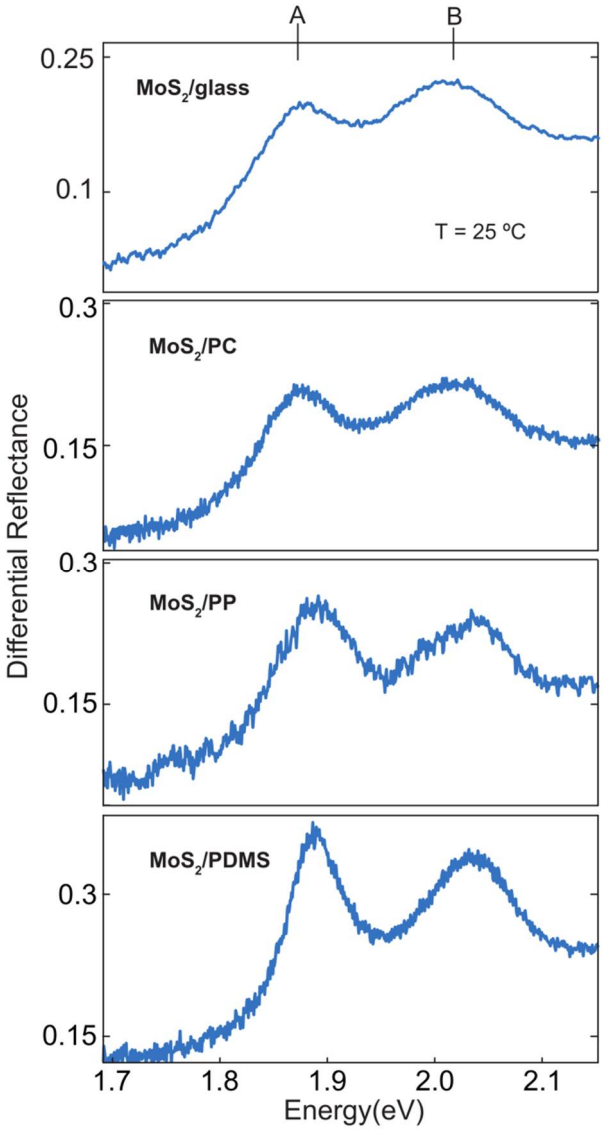

Figure S4. Comparison between the differential reflectance spectra measured for single-layer MoS_2 on different substrates: glass, polycarbonate (PC), polypropylene (PP)and poly-dimethil siloxane (PDMS).

One advantage of choosing PDMS as substrate for the characterization of TMDCs is that once the flakes are fully characterized they can be easily transferred to another substrate by means of an all-dry transfer method that exploits the viscoelasticity of PDMS to accomplish the transfer of the flake.[45] Figure S5 shows some examples of TMDC flakes that have been transferred from the PDMS substrate to a silicon substrate with a 285 nm SiO_2 capping layer, which is one of the standard substrates employed in many laboratories working with graphene and other 2D materials.

Peer-reviewed version available at Nanomaterials 2018, 8, 725; doi:10.3390/nano8090725

For 2D materials supported on SiO_2/Si substrates the quantitative analysis of their optical contrast (defined as $C = (I_{flake}-I_{subs})/(I_{flake}+I_{subs})$) is a common method to identify atomically thin flakes and to estimate their number of layers.[46–52] These analyses are typically carried out by acquiring reflection mode optical images while the illumination wavelength is selected by means of narrow bandpass filters[46,49,50], by hyperspectral imaging [39,53], or by using the micro-reflectance setup employed in this work.[32,33] Figure S6 shows a summary of the optical contrast spectra acquired for MoS_2, WS_2, $MoSe_2$ and WSe_2 flakes with different number of layers. Although this figure could be used as a guide to determine the number of layers of TMDCs exfoliated onto SiO_2/Si substrates, the difference in optical contrast spectra between layers with different thicknesses is more subtle than that measured onto the PDMS substrate by differential reflectance. Also the spectra show a skewed 'S' shape because of the interference color effect, due to the thin SiO_2 dielectric layer on top of the reflective silicon surface, which hampers the identification of the excitonic features that are superimposed (still visible on the MoS_2 flakes, Figure S6a). Therefore, these results illustrate that it is preferable to characterize the TMDCs on the PDMS substrate (by means of the combination of the quantitative analysis of the transmission mode optical images and the differential reflectance/transmittance) prior to their transfer to SiO_2/Si substrates.

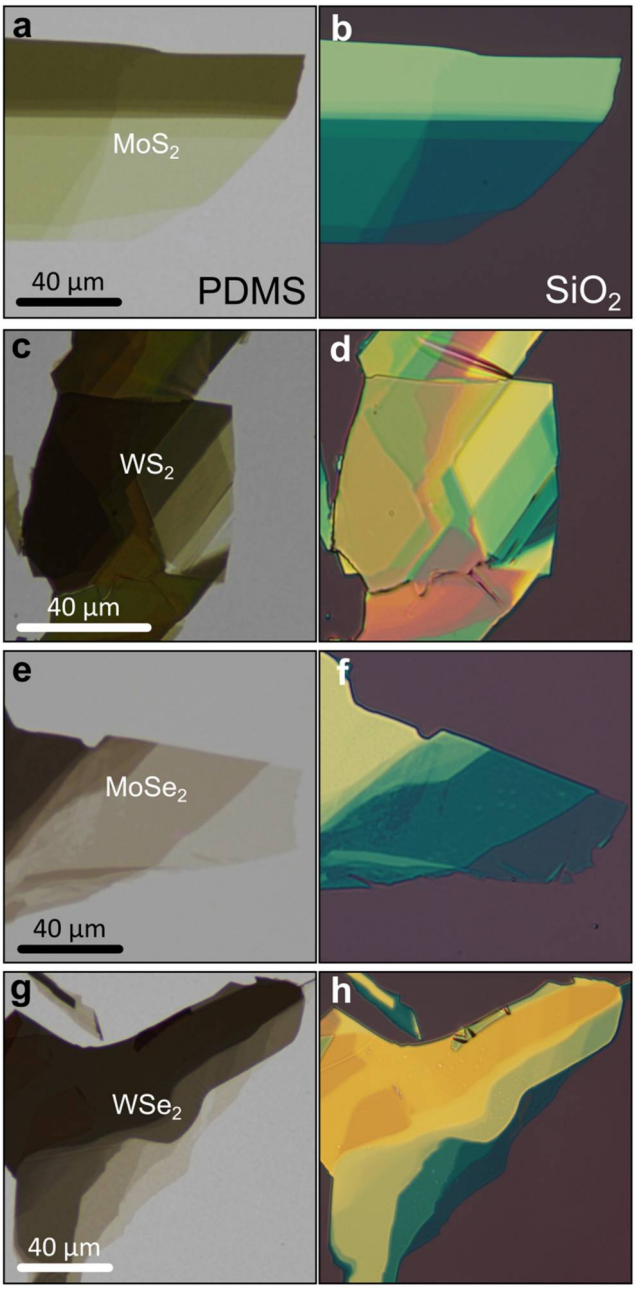

Figure S5. Transmission mode optical images (left panels) of MoS_2 (a), WS_2 (c), $MoSe_2$ (e) and WSe_2 (g) on PDMS substrates. Reflection mode optical images of the same flakes after transfer onto SiO_2/Si substrates (285 nm thick SiO_2): MoS_2 (b), WS_2 (d), $MoSe_2$ (f) and WSe_2 (h). Note: the images on SiO_2/Si substrates have been flipped horizontally to facilitate the comparison with the transmission mode images.

Preprints (www.preprints.org) | NOT PEER-REVIEWED | Posted: 14 August 2018 doi:10.20944/preprints201808.0242.v1

Peer-reviewed version available at Nanomaterials 2018, 8, 725; doi:10.3390/nano8090725

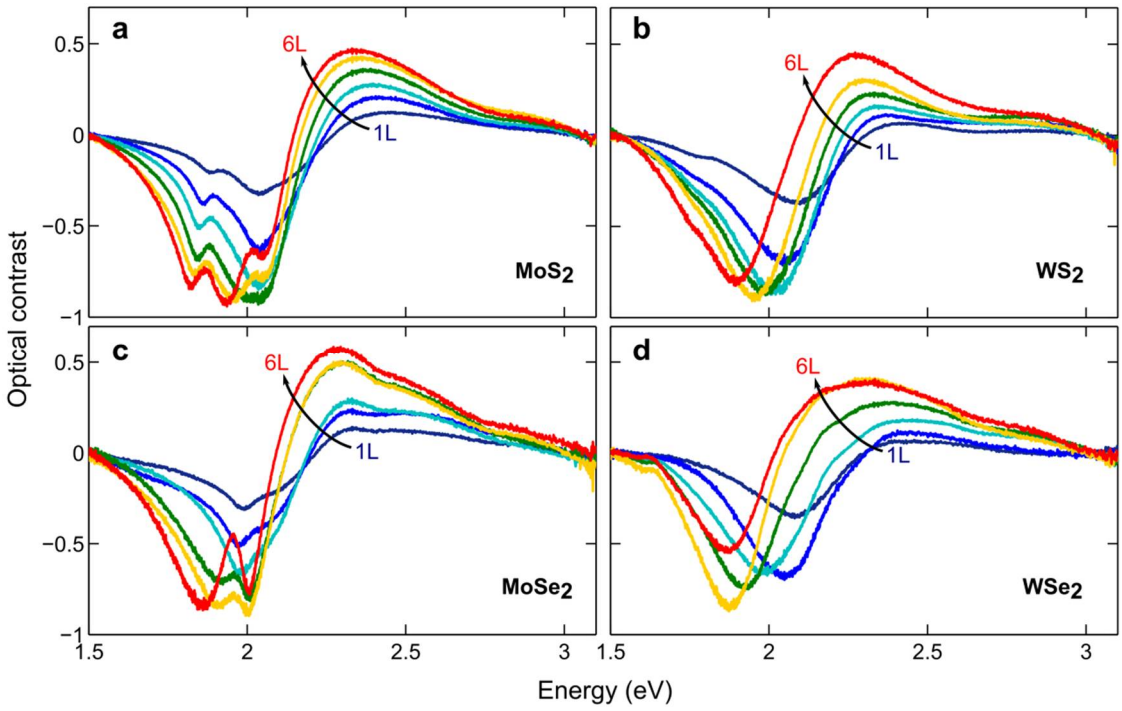

Figure S6. Thickness dependence of the optical contrast measured for MoS_2 (a), WS_2 (b), $MoSe_2$ (c) and WSe_2 (d) deposited onto SiO_2/Si substrates (285 nm thick SiO_2).

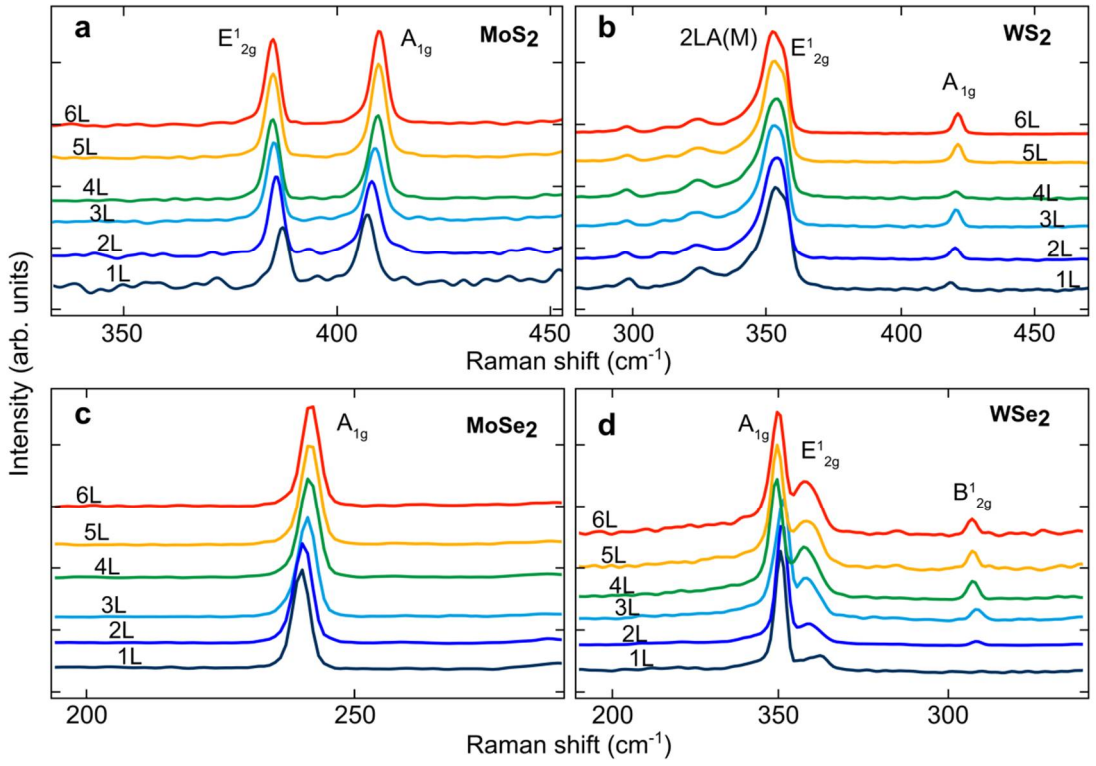

Preprints (www.preprints.org) | NOT PEER-REVIEWED | Posted: 14 August 2018 doi:10.20944/preprints201808.0242.v1

Peer-reviewed version available at Nanomaterials 2018, 8, 725; doi:10.3390/nano8090725

Figure S7. Raman spectra mesured on MoS_2 (a), WS_2 (b), $MoSe_2$ (c) and WSe_2 (d) deposited onto PDMS substrates.

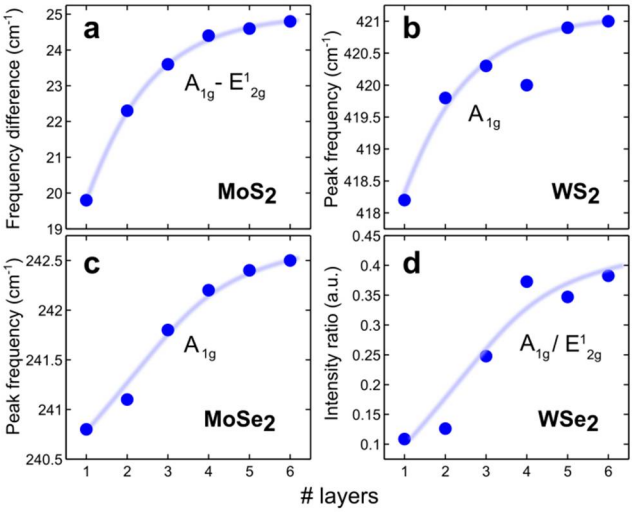

Figure S8. Quantitative analysis of the Raman spectra measured on MoS_2 (a), WS_2 (b), $MoSe_2$ (c) and WSe_2 (d) deposited onto PDMS substrates. The solid lines are guides to the eye.

Preprints (www.preprints.org) | NOT PEER-REVIEWED | Posted: 14 August 2018 doi:10.20944/preprints201808.0242.v1

Peer-reviewed version available at Nanomaterials 2018, 8, 725; doi:10.3390/nano8090725

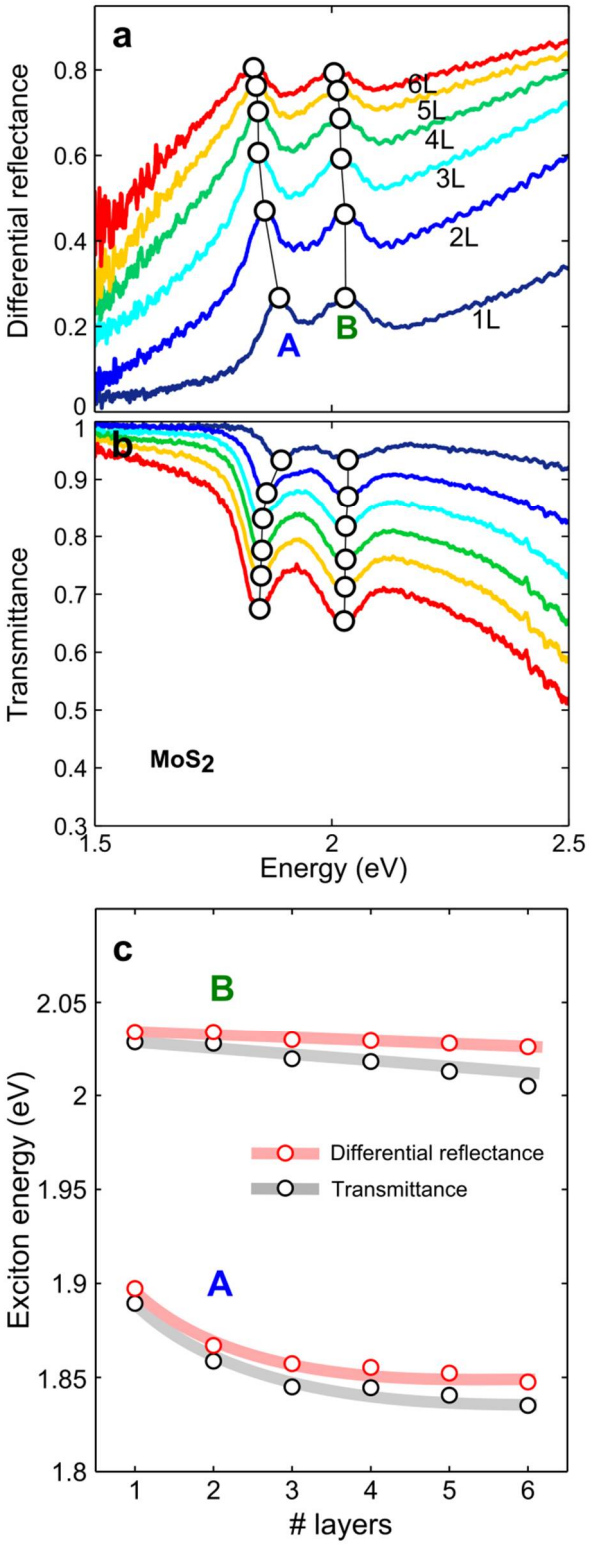

Figure S9. Comparison between differential reflectance (a) and transmittance (b) measurements carried out on the same MoS_2 flakes on PDMS. (c) Comparison between the exciton energies determined from differential reflectance and transmittance measurements. The slight variation between the two methods could be attributed to a slight increase of temperature of the substrate during the transmittance measurements (leading to a slight biaxial straining of the flakes).

Preprints (www.preprints.org) | NOT PEER-REVIEWED | Posted: 14 August 2018 doi:10.20944/preprints201808.0242.v1

Peer-reviewed version available at Nanomaterials 2018, 8, 725; doi:10.3390/nano8090725

Now we turn our attention to the differential reflectance spectra outside the energy window where the exciton resonances occur. We have found that the differential reflectance magnitude increases monotonically with the number of layers. The results are summarized in Figure 7, demonstrating that a quantitative analysis of epi-illumination images can be used to determine the thickness of the MoS_2, $MoSe_2$, WS_2 and WSe_2 samples. The quantitative analysis could be carried out by selecting the illumination wavelength with narrow-bandpass filters, typically used in most laboratories to enhance the optical contrast of 2D materials.

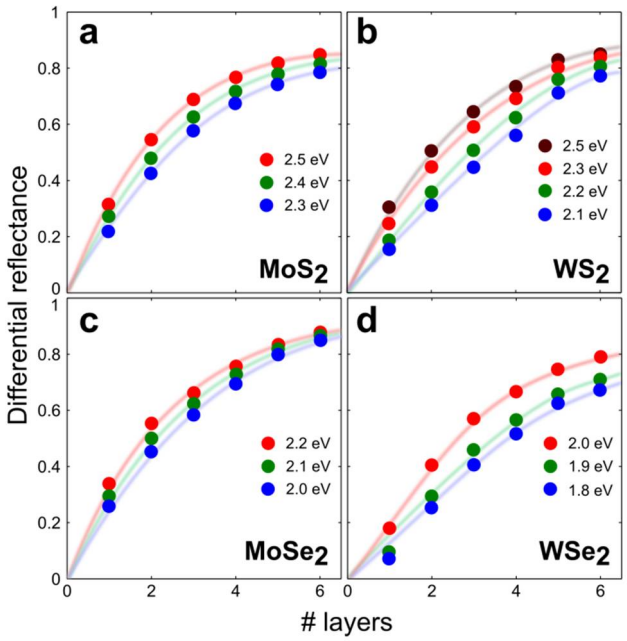

Figure S10. Differential reflectance intensity measured from the differential reflectance spectra shown in Figure S6 at energies outside the excitonic resonance windows: (a) MoS_2, (b) WS_2, (c) $MoSe_2$ and (d) WSe_2. The solid lines are guides to the eye.

Preprints (www.preprints.org) | NOT PEER-REVIEWED | Posted: 14 August 2018 doi:10.20944/preprints201808.0242.v1

Peer-reviewed version available at Nanomaterials 2018, 8, 725; doi:10.3390/nano8090725

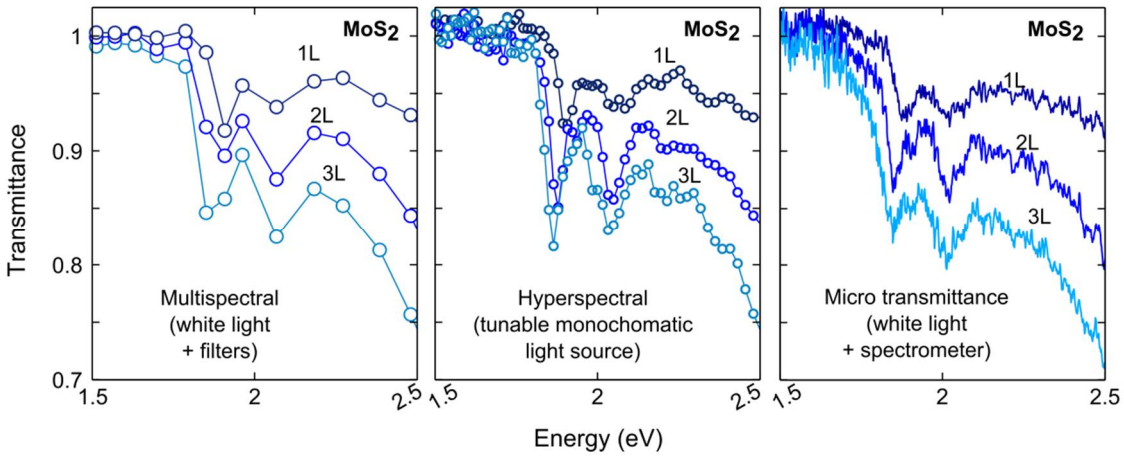

Figure S10. Comparison between different methods to measure the optical properties of 2D materials (using 1L, 2L and 3L MoS_2 as testbed). In the multispectral measurements narrow bandwidth filters are used to select the illumination wavelength. In the hyperspectral method the illumination is carried out through a white-light source connected to a monochromator. In the micro-transmittance measurement, we employ white light, which is collected through an optical fiber (acting as a confocal pinhole) and sent to a CCD spectrometer.

Figure S11 shows an artistic representation of the crystal structure of 2H- (Figure S11 up) and 3R- (Figure S11 down) MX_2 crystals. The 2H and 3R phase differ in the bulk crystals, since it arises from a different stacking of 2D layers, interacting by van der Waals forces. For instance, in MoS_2, the 2H phase presents unit cell parameters $a = b = 3.1625$ Å and c = 12.300 Å (space group $P6_3/mmc$), while the 3R phase presents unit cell parameters $a = b = 3.1607$ Å and c = 18.344 Å (space group $R3m$).[1]

The different stacking of the 2H and the 3R phase leads to slightly distinct band structures and, therefore, different excitonic phenomena. In the case of MoS_2, for example, the energy splitting of the top of the valence band at the $\overline{K}$ point is smaller for the 3R-MoS_2 (0.14 eV) than for the 2H-MoS_2 (0.17 eV), which is translated in different exciton splitting [2]. This different splitting can be observed in the differential reflectance spectra (Figure S14 and Figure S15). In Figure S12 we show optical microscopy images of mechanically exfoliated flakes of 2H- and 3R- MoS_2 mono- and few-layer crystals on a PDMS substrate, where no difference can be depicted between the two phases. Also, the transmittance extracted from transmission mode images seems very similar for both 2H and 3R polytypes (Figure S13). Therefore, the quantitative analysis of the A and B exciton energy difference seems the more reliable way to distinguish between the 2H and the 3R polytypes.

Preprints (www.preprints.org) | NOT PEER-REVIEWED | Posted: 14 August 2018 doi:10.20944/preprints201808.0242.v1

Peer-reviewed version available at Nanomaterials 2018, 8, 725; doi:10.3390/nano8090725

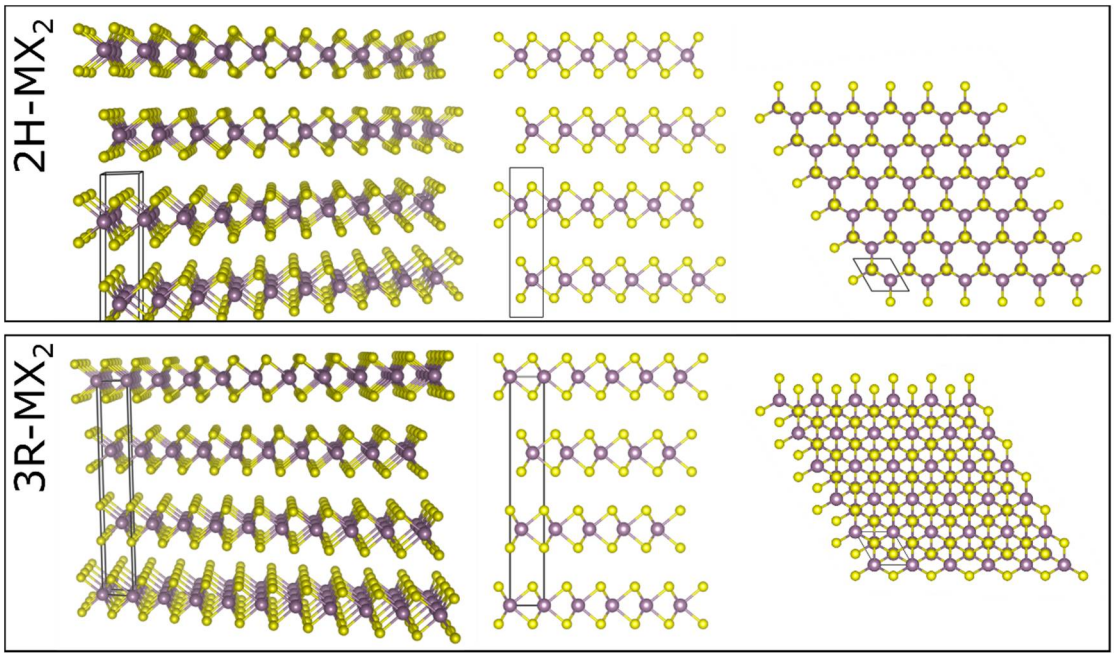

Figure S11. Comparison between the crystal structure of the 2H- and 3R- polytypes.

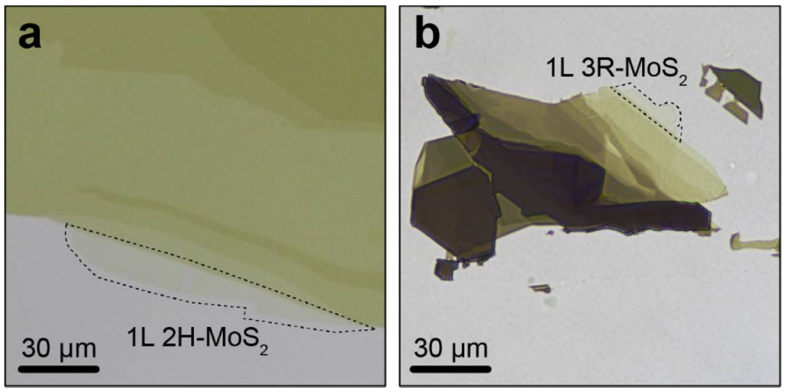

Figure S12. Transmission mode optical images of 2H-MoS_2 (a) and 3R-MoS_2 on PDMS. The dashed regions highlight the single-layer regions. Note that MoS_2 single-layers of 2H and 3R have the same structure and they only differ for multilayered stacks.

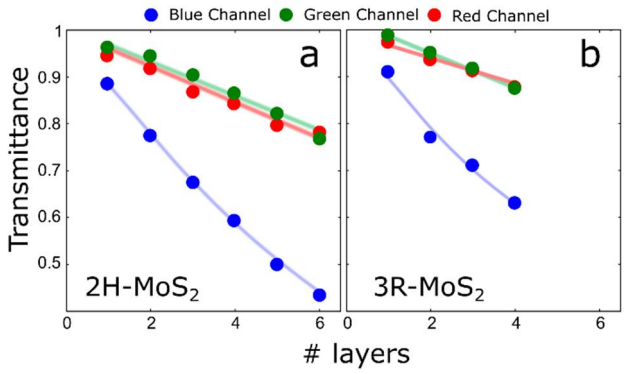

Figure S13. Transmittance (extracted from the red, green and blue channels of the trasnmission mode optical images) as a function of the number of layers for (a) 2H-MoS_2 and (b) 3R-MoS_2. The solid lines are guides to the eye.

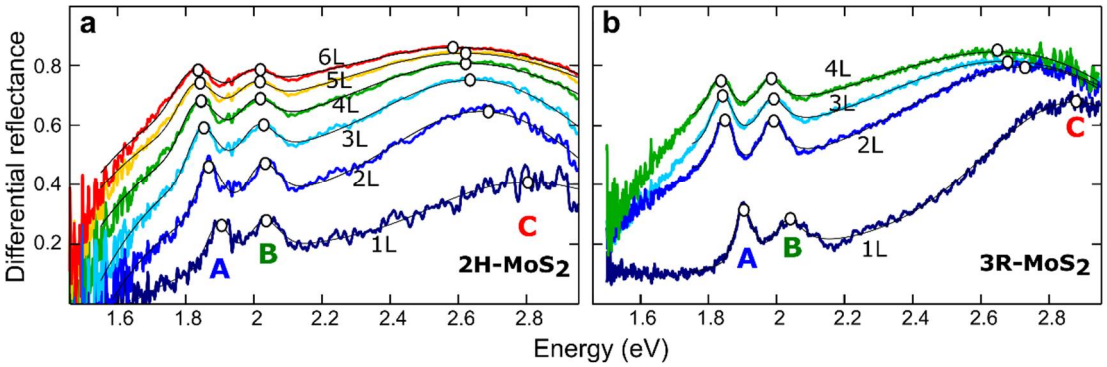

Figure S14. Differential reflectance spectra measured as a function of the number of layers for (a) 2H-MoS_2, (b) 3R-MoS_2. The spectra have been fitted to a sum of Lorentzian/Gaussian peaks (solid thin black lines) to determine the position of the different excitonic features (highlighted with white circles).

Preprints (www.preprints.org) | NOT PEER-REVIEWED | Posted: 14 August 2018 doi:10.20944/preprints201808.0242.v1

Peer-reviewed version available at Nanomaterials 2018, 8, 725; doi:10.3390/nano8090725

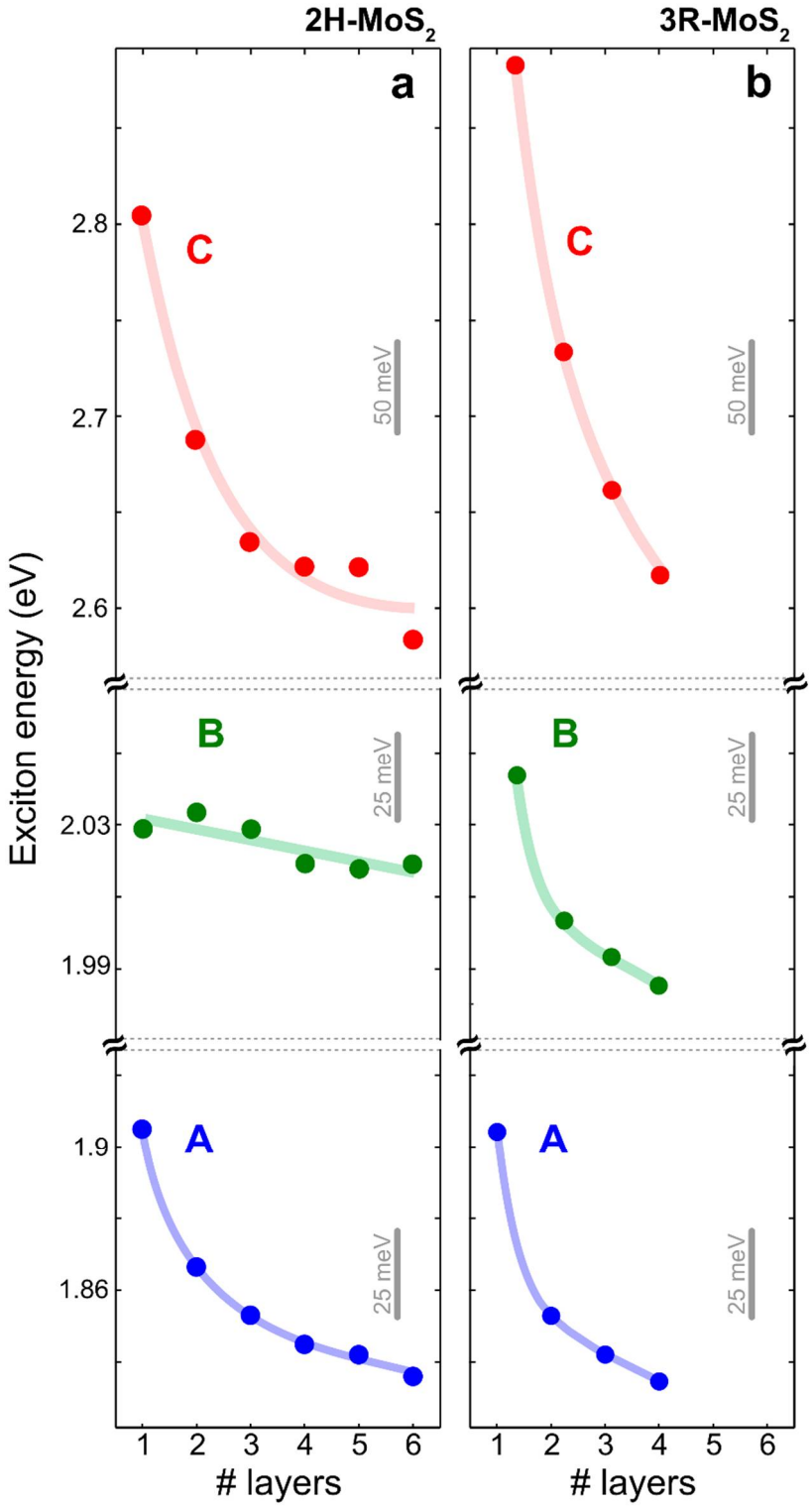

Figure S15. Thickness dependence of the exciton energies, extracted from the differential reflectance spectra of (a) 2H-MoS_2 and (b) 3R-MoS_2. The solid lines are guides to the eye.

Details on the *ab initio* calculations:

All calculations are performed using a code written on our own [3].

Peer-reviewed version available at Nanomaterials 2018, 8, 725; doi:10.3390/nano8090725

To end up with the absorption spectra of the four different TMDCs, we start with a DFT calculation in the LDA approximation using three shells of localized Gaussian orbitals as basis set. Each of the shells is composed of ten orbital functions covering the symmetries s, p, d and s^*. All orbitals inside one shell share the same material dependent decay constant, which are in a range of $0.13\ a_B^{-2}$ to $2.5\ a_B^{-2}$. The reciprocal space is sampled with a $12 \times 12 \times 1$ k-point grid for the mono- and bilayers and a $10 \times 10 \times 3$ k-point grid for the bulk crystals. We use the structural parameters as reported in Ref. [4] (for MoS_2 and $MoSe_2$) and Ref. [5] (for WS_2 and WSe_2) with experimental lattice constants of 3.160 Å, 3.299 Å, 3.155 Å and 3.286 Å for MoS_2, $MoSe_2$, WS_2 and WSe_2, respectively. The S or Se atoms of the mono- and bilayer system from neighboring unit cells are vertically separated by at least 28 Å vacuum to suppress interactions due to the periodic continuation perpendicular to the layers (in the DFT). Spin-orbit interaction is included in terms of corresponding pseudopotentials and all spin-split bands enter in the consecutive quasiparticle calculation.

The quasiparticle corrections are calculated within the LDA+GdW [6] approximation, which allows for well converged results at comparably low numerical costs. Figure S16 shows the convergence behavior of the direct gaps at the high symmetry point K with respect to the auxiliary plane wave basis to represent ε and W. For this convergence study, the k-point grid is chosen as $12 \times 12 \times 1$ for the mono- and bilayers and $12 \times 12 \times 3$ for the bulk crystals. The data in Figure S1 show that a plane wave basis of 2.5 Ry (205 plane waves) is already sufficient. At both levels, DFT and GW, the spin-orbit interaction is fully taken into account.

In order to get the absorption spectra we solve the Bethe-Salpeter equation (BSE) using identical k-point grids for the quasiparticle corrections and the electron-hole interactions therefore avoiding the need of an interpolation scheme. The A exciton is the lowest optically bright excitation. The B exciton corresponds to the next optically bright excitation that is not an excited state of the A exciton. Figure S17 and Figure S18 summarize the convergence of the A and B excitons. Apparently, a k-point grid of $24\times 24 \times 1$ (mono-/bilayer) or $18 \times 18 \times 3$ (bulk) yields well-converged results. These k-point grids are employed for the data shown in Figure S19 and

Preprints (www.preprints.org) | NOT PEER-REVIEWED | Posted: 14 August 2018 doi:10.20944/preprints201808.0242.v1

Peer-reviewed version available at Nanomaterials 2018, 8, 725; doi:10.3390/nano8090725

Figure S20. Since the C (D) exciton is composed of several excitations, we calculate the excitation energy as a weighted sum over all excitations inside an energy window that is chosen such that the leading and tailing edges of the peaks are dropped equally to the level of the absorption background (see Figure S19 for more details). To account for uncertainties in the definition of the C (D) exciton, we introduce an error in the respective energetic positions. For the monolayers we include four valence and six conduction bands, while for the bilayer and bulk crystals these numbers are doubled (since the number of atoms in the unit cell are doubled).

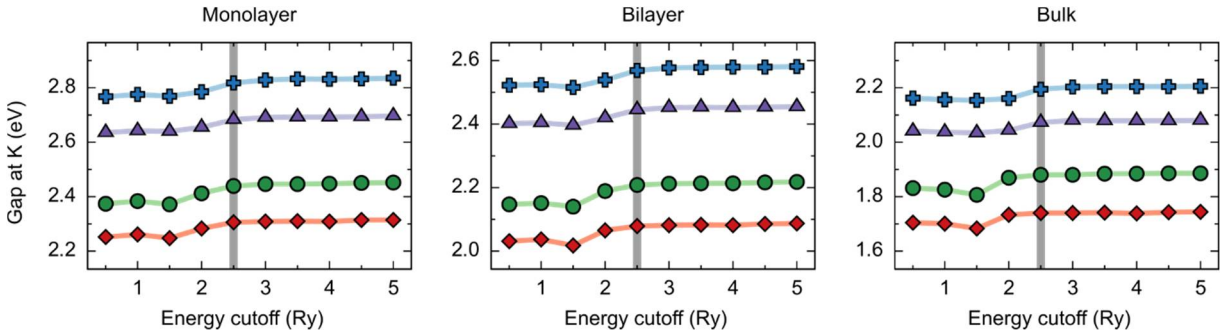

Figure S16. Convergence of the quasiparticle gap at the K point with respect to the energy cutoff used in the LDA+GdW approach for the representation of ε and W. For the mono- and bilayers a k-point grid of $12 \times 12 \times 1$ and for the bulk crystals a k-point grid of $12 \times 12 \times 3$ is used. All four materials MoS_2 (✚), $MoSe_2$ (●), WSe_2 (◆) and WS_2 (▲) show similar convergence behaviour for all three numbers of layers. The grey line shows the chosen energy cutoff of 2.5 Ry employed for preparing the subsequent BSE calculations.

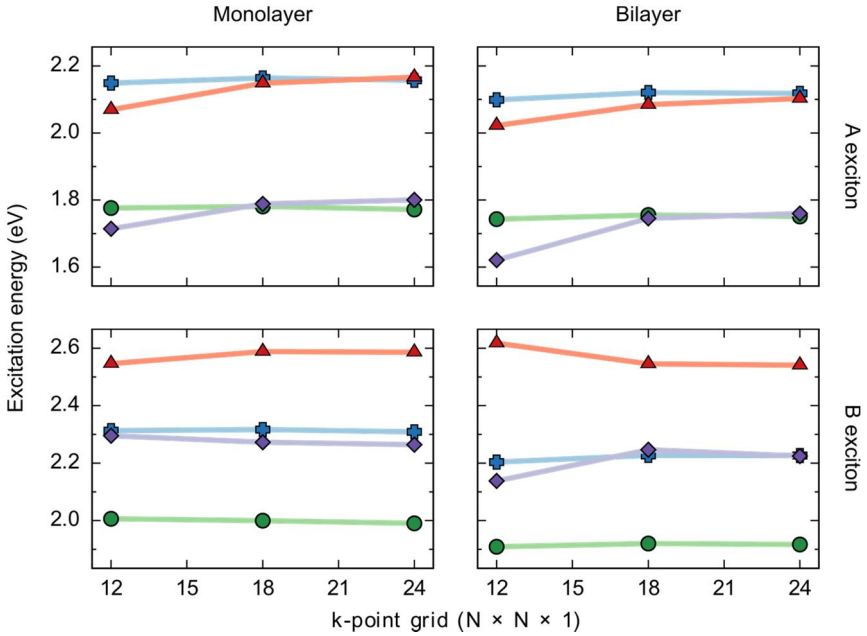

Preprints (www.preprints.org) | NOT PEER-REVIEWED | Posted: 14 August 2018 doi:10.20944/preprints201808.0242.v1

Peer-reviewed version available at Nanomaterials 2018, 8, 725; doi:10.3390/nano8090725

Figure S17. Convergence of the A and B exciton for all four TMDCs MoS_2 (✚), $MoSe_2$ (●), WS_2 (▲) and WSe_2 (◆) with respect to the k-point grid used in the BSE. For the monolayers four valence and six conduction bands are included and for the bilayers eight valence and twelve conduction bands were taken into account. The solid lines are guides to the eye.

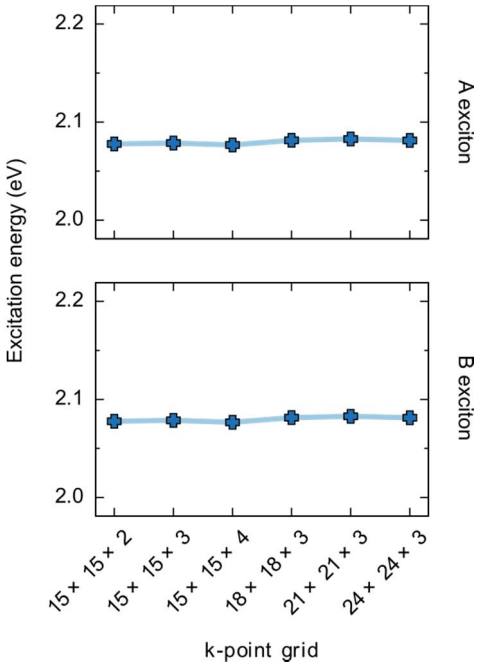

Figure S18. Convergence of the A and B exciton for the bulk crystal of MoS_2 with respect to the k-point grid applied in the BSE. Note that the number of bands were reduced to four valence and six conduction bands for these calculations to facilitate the calculation with $24 \times 24 \times 3$ k-points. The solid lines are guides to the eye.

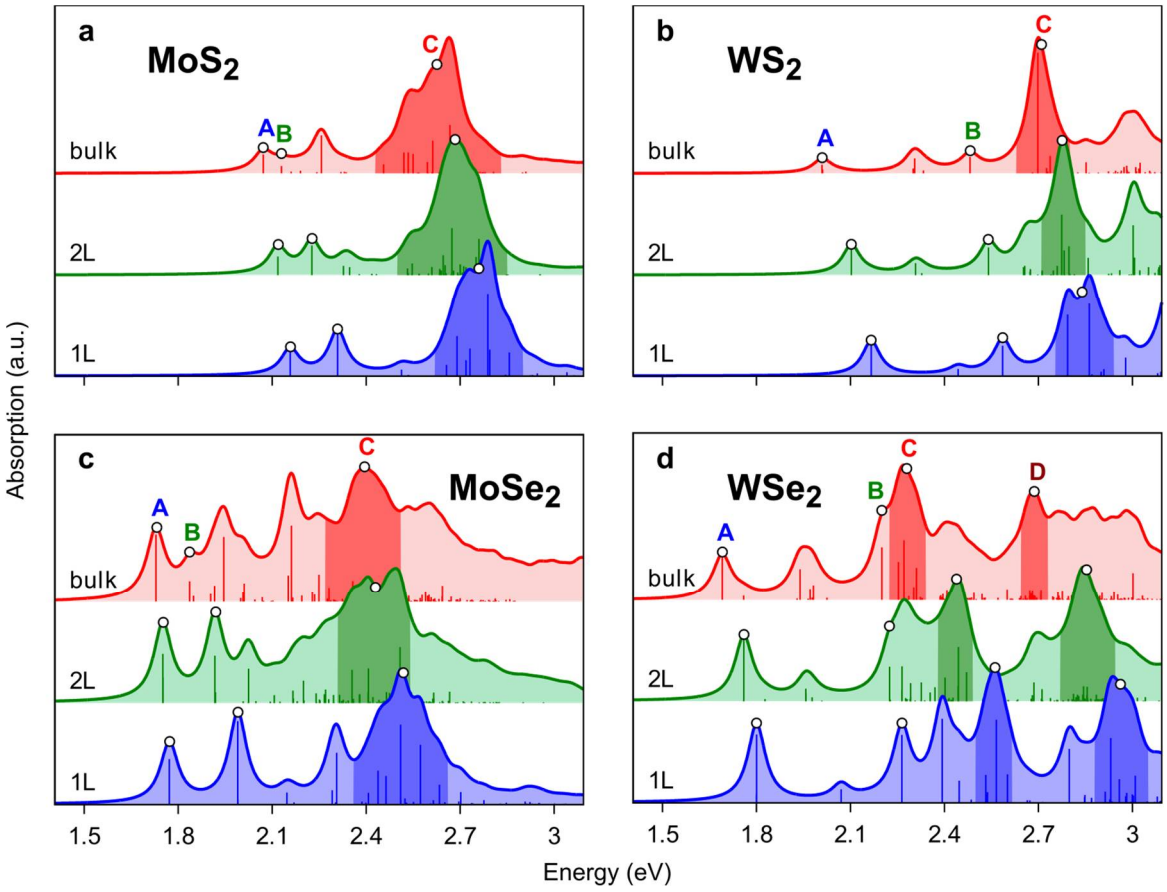

Figure S19. Absorption spectra of MoS_2 (**a**), WS_2 (**b**), $MoSe_2$ (**c**) and WSe_2 (**d**) for all studied number of layers. An artificial broadening of 35 meV is introduced and the spectra are vertically shifted to distinguish between the different systems of one material. The energy window chosen for the weighted sum of the respective C and D excitons are marked by the darker regions of the spectra.

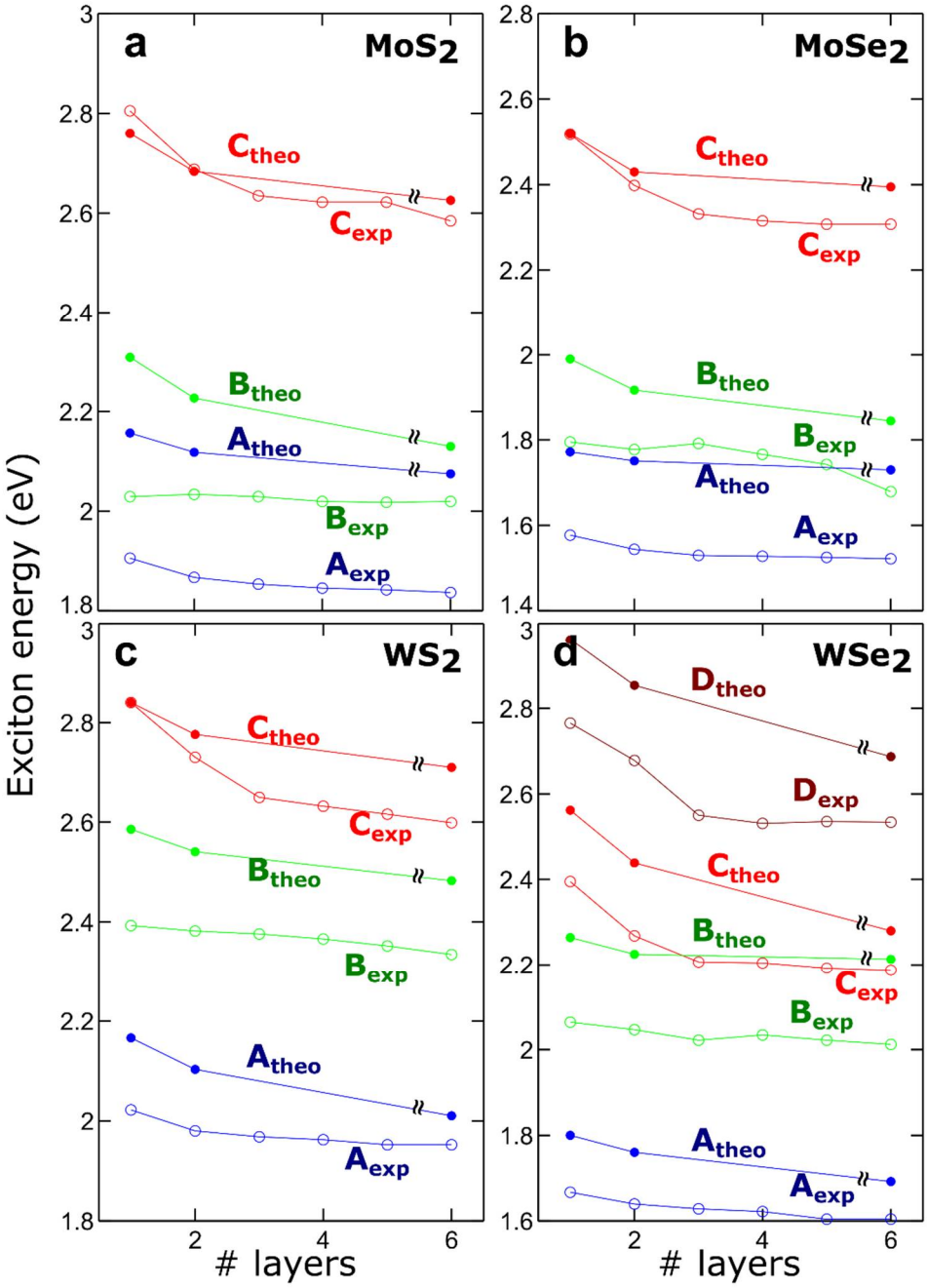

Figure S20. Direct comparison between the exciton energies obtained experimentally and those calculated for MoS_2 (**a**), WS_2 (**b**), $MoSe_2$ (**c**) and WSe_2 (**d**).

SUPP. INFO. REFERENCES

(1) Schönfeld, B., Huang, J. J., & Moss, S. C. Anisotropic mean-square displacements (MSD) in single-crystals of 2H-and 3R-MoS2. *Acta Crystallographica Section B: Structural Science* **1983**, *39*(4), 404-407.

(2) Suzuki, R., *et al*. Valley-dependent spin polarization in bulk MoS2 with broken inversion symmetry. *Nature Nanotechnology*, **2014** *9*(8), 611-617.

(3) Rohlfing, M.; Krüger, P.; Pollmann, J. Quasiparticle band-structure calculations for C, Si, Ge, GaAs, and SiC using Gaussian-orbital basis sets. *Phys. Rev. B* **1993**, *48*, 17791-17805.

(4) Böker, T.; Severin, R.; Müller, A.; Janowitz, C.; Manzke, R.; Voß, D.; Krüger, P.; Mazur, A.; Pollmann, J. Band Structure of MoS_2, $MoSe_2$, and α−$MoTe_2$: Angle-Resolved Photoelectron Spectroscopy and *ab initio* Calculations. *Phys. Rev. B* **2001**, *64*, 235305.

(5) Yun, W. S.; Han, S. W.; Hong, S. C.; Kim, I. G.; Lee, J. D. Thickness and Strain Effects on Electronic Structures of Transition Metal Dichalcogenides: 2H-MX_2 Semiconductors (M = Mo, W; X = S, Se, Te). *Phys. Rev. B* **2012**, *85*, 33305.

(6) Rohlfing, M. Electronic Excitations from a Perturbative LDA+*GdW* Approach. *Phys. Rev. B* **2010**, *82*, 205127.